Inclusive UPC charm photoproduction in ALICE

S. Nese[a] for the ALICE collaboration
Department of Physics, University of Oslo, Norway

Ultra-peripheral heavy-ion collisions provide an opportunity to use inelastically photoproduced charm to study the nuclear gluon distribution. In these collisions, a photon emitted from one nucleus interacts with a gluon in the target nucleus, producing a charm anti-charm quark pair. These fragment to open- or hidden-charm hadrons, which are reconstructed. The transverse momentum distribution for photoproduced D^0 mesons are presented, and the results compared to model calculations.

DOI: https://doi.org/10.17161/a5fzxf11
Keywords: ultra-peripheral collisions, photonuclear interactions, photoproduction of charm, D^0 mesons

1 Introduction

In ultra-peripheral collisions of heavy ions (UPC), charm-anticharm quark pairs are predominantly produced through the interaction of a photon from the emitter nucleus with a single parton in the target nucleus, e.g. $\gamma + g \rightarrow c\bar{c}$, as illustrated in Fig. 1. The charm quarks hadronize, emerging as open- or hidden-charm hadrons in the detector. Such events therefore give access to the gluon distribution of the target, reaching Bjorken-x values of $\sim 10^{-4}$. Measurements of inelastically photoproduced charm hadrons in UPC are therefore sensitive to nuclear effects such as saturation and shadowing. Moreover, simulations of open charm photoproduction using the Pythia 8 Angantyr model [1,2] indicate that compared to the p_{T}-integrated spectrum, the distribution of probed gluons have lower mean values of Bjorken-x for low-p_{T} hadrons.

In general, due to the exchange of a colored parton, the target breaks up and produces a shower of hadrons. Meanwhile, the emitter nucleus stays intact. Therefore, charm photoproduction events are characterized by large regions devoid of particle production on the photon-going side, while the target-going side sees particle production in the forward region. Such single rapidity-gap events are copiously produced in Pb—Pb collisions at the LHC, and recorded in ALICE for the first time during the Run 3 data-taking campaign.

In this presentation, which is an update of a previous study [3], photoproduction of D^0 mesons will be discussed.

2 Measurement of photoproduced D^0 in UPC using ALICE

2.1 Selection of inelastic UPC events

During Run 3 of the LHC, ALICE uses a streaming readout system for the collection of data from heavy-ion collisions. With an interaction rate of up to 50 kHz [4], large numbers of inelastic UPC events are recorded. These events are identified offline by a rapidity gap selection algorithm. The photon from the

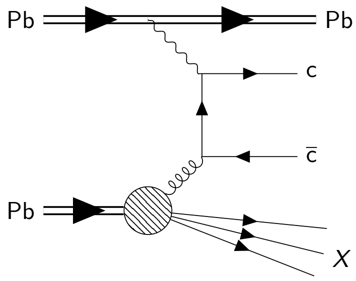

Figure 1: Representative diagram for the inelastic photoproduction of charm in UPC.

[a]Speaker, email: sinese@cern.ch

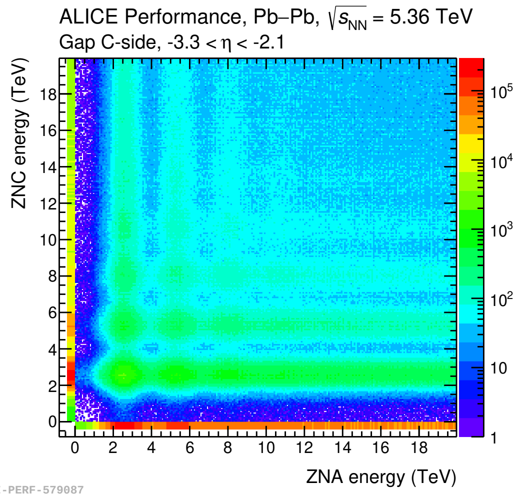

Figure 2: Energy deposited in the ZNA vs. energy deposited in ZNC, in events selected as having a rapidity gap on the $-\eta$ side. The peaks correspond to specific numbers of neutrons. Events with no energy deposited in one of the neutron calorimeters are shown in the underflow bins below zero.

emitter nucleus has a relatively low energy compared to the target nucleon, which results in the particle production from the inelastic process being shifted towards the target-going direction. Therefore, at large absolute values of pseudorapidity η, the event will show a characteristic asymmetry, with the photon-going side being devoid of particles, while there is some particle production in the target-going side. Selection of single rapidity-gap events is performed using the ALICE Fast Interaction Trigger detectors, which are positioned on either side of the interaction point at large $|\eta|$. Events are required to have a signal below a set threshold on one side of the interaction point, while having a signal above the threshold on the opposite side. These sides are then identified as the photon-going direction and the target-going direction, respectively. For the current analysis, the FIT FT0 is used to perfom the rapidity-gap selection. The FT0 consists of two quartz Cherenkov radiator arrays, covering pseudorapidities of $3.5 < \eta < 4.9$ for the FT0-A and $-3.3 < \eta < -2.1$ for the FT0-C [5].

In inelastic UPC events, there is a high probability of breakup of the target nucleus, resulting in the emission of neutrons. Meanwhile, the emitter nucleus stays has a high probabilty of staying intact. Therefore, to obtain a purer sample of inelastic events, the ALICE Zero-Degree Calorimeters (ZDC) are used to detect (the absence of) nuclear breakup. The ZDC detectors are placed 112.5 meters from the interaction point along the z-axis in both directions, and consist of proton calorimeters and neutron calorimeters [6]. In this analysis, the neutron calorimeters (ZNA and ZNC) are used to detect neutrons emitted from the target nucleus. The selection follows a similar logic as the rapidity-gap selection, with a requirement of at least one neutron (Xn) on the target-going side, while the photon-going side is required to have no neutrons detected (0n). Fig. 2 shows the energies measured by the ZNA and ZNC, in events classified as having a rapidity gap on the $-\eta$ side. Peaks for one or more neutrons can be identified. As expected, the energies measured on the $-\eta$ side (ZNC) are biased towards lower values, while the opposite side (ZNA), where no rapidity gap is measured, has a flatter distribution of neutrons.

2.2 Reconstruction of charm hadrons

D^0 mesons are reconstructed in their decay mode to charged hadrons, $D^0 \to K^-\pi^+$. The reconstruction is done at midrapidity ($|y| < 0.9$) using tracks measured by the Time Projection Chamber (TPC). In addition to providing three-dimensional tracking for charged particles, the TPC is also used in this analysis to identify kaons by measuring specific energy loss (dE/dx) [7,8]. To further reduce background, kaon candidates are also required to pass a particle identification selection based on velocity measured by the Time Of Flight (TOF) detector [9].

The charm decay vertex is reconstructed in the ALICE Inner Tracking System (ITS). In Run 3, the ITS consists of 7 layers of monolithic active pixel sensors placed at radial distances of 22 mm to 400 mm from the interaction point [10]. Given the primary and secondary vertices, both the decay length as well as the alignment between candidate momentum and the displacement vector can be extracted. This allows

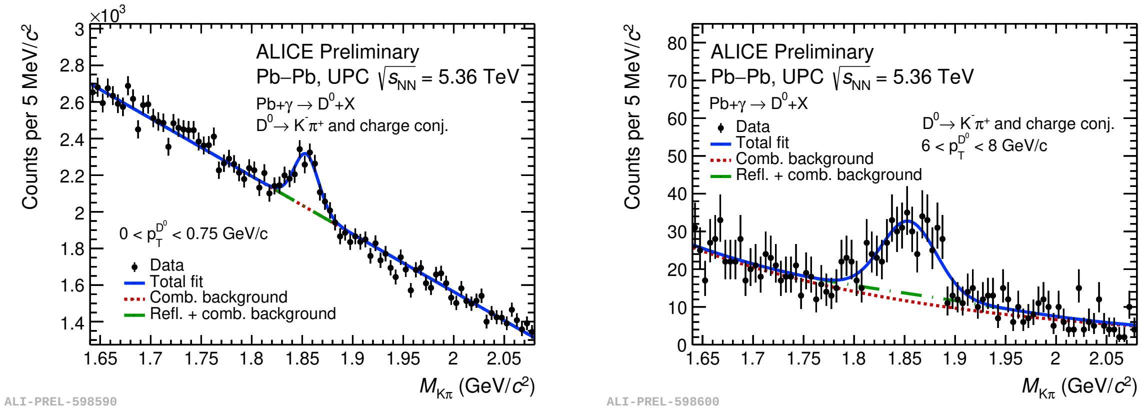

(a) (b)

Figure 3: Fits to the invariant mass of D^0 daughter pair candidates, in events with a rapidity gap on the $-\eta$ side. (a): D^0 candidate p_T from 0 to $0.75\,\mathrm{GeV}/c$. (b): D^0 candidate p_T from $6\,\mathrm{GeV}/c$ to $8\,\mathrm{GeV}/c$.

for an improvement of the D-meson signal significance by applying topological cuts.

The D^0 signal is extracted as a function of p_T by fitting a signal-background functional form to the invariant mass distributions of daughter pair candidates. This is done in 8 bins of p_T from 0 to $12\,\mathrm{GeV}/c$. Two example bins are shown in Fig. 3 for the class of events with the photon-going direction identifed as the $-\eta$ side. The fit consists of a signal component, a combinatorial background component, and a correlated background due to the swapped mass assignments of the $K^{\pm}$ and $\pi^{\pm}$. For the correlated background, Monte-Carlo simulations are used to fix the shape and relative normalization.

To obtain the p_T distribution of photoproduced D^0, a correction for acceptance and efficiency is applied to the raw yield distribution. This correction is calculated using Monte-Carlo simulations, where STARlight [11] provides the photon spectrum, and DPMJET [12] generates the photoproduced charm hadron. The final state particles are propagated through the ALICE detector using GEANT4 [13].

3 Results

Results were obtained separately for events with photon going in the $+\eta$ and $-\eta$ directions. The corrected p_T distributions for photoproduced D^0 are shown for the two event classes in Fig. 4a. The distributions are normalized by the number of visible events, i.e. the number of events passing the rapidity-gap and neutron class selections described in Section 2.1.

The p_T distribution is not expected to be strongly dependent on the size of the rapidity gap. Therefore, the two event classes, corresponding to single rapidity-gap events as measured by the FT0-A or FT0-C, are combined for the purpose of comparisons with theoretical calculations and other measurements. The mean p_T of the resulting distribution is $1.476 \pm 0.026\ (\mathrm{stat}) \pm 0.048\ (\mathrm{syst.})\ \mathrm{GeV}/c$. The combined p_T distribution is shown in Fig 4b.

The measurement of photoproduced D^0 in high granularity down to $p_T = 0$ allows for a comparison of the shape of the p_T distribution to theoretical model calculations. To facilitate this, all histograms and curves in Fig. 4b are normalized to the same integrated yield. The results are compared to three calculations in the Color Glass Condensate framework. The calculation by Gimeno-Estivill et al. [14] qualitatively desribes the measured shape above $1\,\mathrm{GeV}/c$, but underpredicts the mean p_T. Meanwhile, both calculations by Gonçalves et al. [15] overpredict the mean p_T. The measured p_T shape is consistent with that of the cross section measurement by the CMS Collaboration [16].

The charm (anti-)quark produced in the hard scattering may hadronize into other meson states in addition to the D^0. Using the same event selections as for the D^0 analysis, D^+ and D^{*+} were reconstructed in the decay modes $D^+ \rightarrow K^-\pi^+\pi^+$ and $D^{*+} \rightarrow D^0\pi^+ \rightarrow K^-\pi^+\pi^+$. The corresponding invariant mass distributions, integrated over p_T, are shown in Fig 5a and 5b, respectively. Measurements of several charm channels in inelastic UPC provides a new avenue to study the system dependence of charm hadronization.

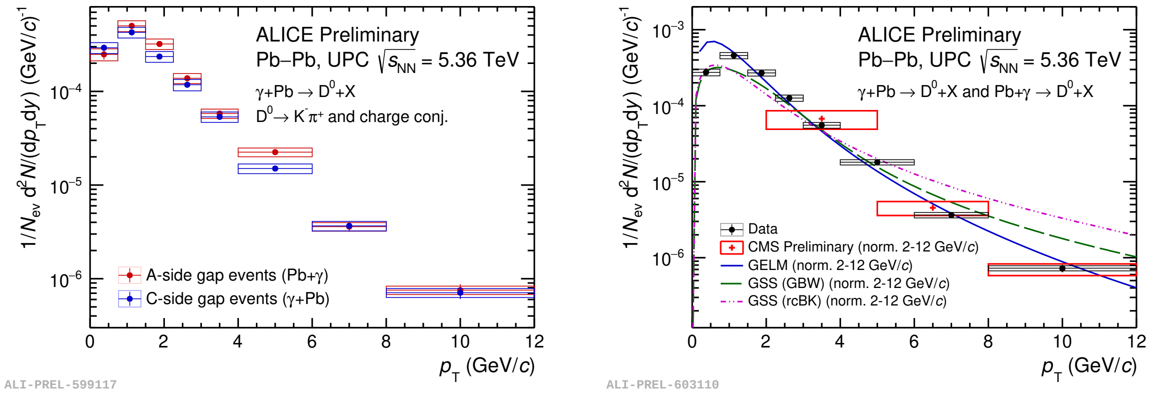

(a) (b)

Figure 4: (a): Corrected p_{T} distribution of photoproduced D^0 for events with the photon-going direction towards $+\eta$ (red) and $-\eta$ (blue). (b): Combined p_{T} distribution for both single rapidity-gap event classes. Also shown are theoretical results in the Color-Glass-Condensate framework, and the CMS preliminary cross section measurement. This note is an update of a previous study [3].

4 Summary and Outlook

ALICE has measured the p_{T} distribution of photoproduced D^0 in UPC down to $p_{\mathrm{T}} = 0$ for the first time. Upcoming D^0 cross section measurments in ALICE will act as a probe of the nuclear gluon distribution, with the low p_{T} mesons providing the highest sensitivity to the low-x region. D^+ and D^{*+} were also reconstructed in inelastic UPC, pointing to new possibilities of investigating the system dependence of charm hadronization.

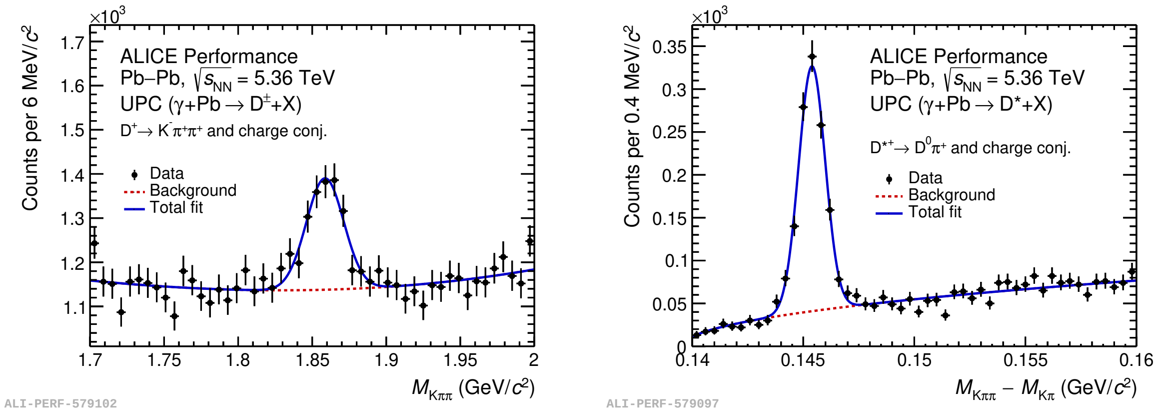

(a) (b)

Figure 5: (a): Invariant mass distribution of D^+ candidates. (b): Invariant mass distribution of D^{*+} candidates.

References

1. C. Bierlich, S. Chakraborty, N. Desai, L. Gellersen, I. Helenius, P. Ilten, L. Lönnblad, S. Mrenna, S. Prestel and C. T. Preuss, *et al.* “A comprehensive guide to the physics and usage of PYTHIA 8.3,” SciPost Phys. Codeb. **2022** (2022), 8 doi:10.21468/SciPostPhysCodeb.8
2. C. Bierlich, G. Gustafson, L. Lönnblad and H. Shah, “The Angantyr model for Heavy-Ion Collisions in PYTHIA8,” JHEP **10** (2018), 134 doi:10.1007/JHEP10(2018)134
3. S. Nese [ALICE], “New probes of nuclear gluon dynamics through photoproduction of charm in

inelastic ultra-peripheral Pb—Pb collisions with ALICE," [arXiv:2509.11814 [nucl-ex]].
4. ALICE Collaboration, "ALICE upgrades during the LHC Long Shutdown 2," JINST **19**, no.05, P05062 (2024) doi:10.1088/1748-0221/19/05/P05062
5. W. H. Trzaska [ALICE], "New Fast Interaction Trigger for ALICE," Nucl. Instrum. Meth. A **845**, 463-466 (2017) doi:10.1016/j.nima.2016.06.029
6. C. Oppedisano, R. Arnaldi, E. Chiavassa, C. Cicalo, P. Cortese, A. De Falco, G. Dellacasa, N. De Marco, A. Ferretti and M. Floris, *et al.* "Physics performance of the ALICE zero degree calorimeter," Nucl. Phys. B Proc. Suppl. **197**, 206-210 (2009) doi:10.1016/j.nuclphysbps.2009.10.068
7. J. Alme *et al.* "The ALICE TPC, a large 3-dimensional tracking device with fast readout for ultra-high multiplicity events," Nukl. Instrum. Meth. A **622**, 316-367 (2010) doi:10.1016/j.nima.2010.04.042
8. ALICE Collaboration, "Upgrade of the ALICE Time Projection Chamber," CERN-LHCC-2013-020.
9. ALICE Collaboration "ALICE technical design report of the time-of-flight system (TOF)," CERN-LHCC-2000-012.
10. B. Abelev *et al.* [ALICE], "Technical Design Report for the Upgrade of the ALICE Inner Tracking System," J. Phys. G **41**, 087002 (2014) doi:10.1088/0954-3899/41/8/087002
11. S. R. Klein, J. Nystrand, J. Seger, Y. Gorbunov and J. Butterworth, "STARlight: A Monte Carlo simulation program for ultra-peripheral collisions of relativistic ions," Comput. Phys. Commun. **212**, 258-268 (2017) doi:10.1016/j.cpc.2016.10.016
12. R. Engel, "Photoproduction within the two component dual parton model. 1. Amplitudes and cross-sections," Z. Phys. C **66**, 203-214 (1995) doi:10.1007/BF01496594
13. S. Agostinelli *et al.* [GEANT4], Nucl. Instrum. Meth. A **506** (2003), 250-303 doi:10.1016/S0168-9002(03)01368-8
14. P. Gimeno-Estivill, T. Lappi and H. Mäntysaari, "Inclusive D0 photoproduction in ultraperipheral collisions," Phys. Rev. D **111** (2025) no.11, 114036 doi:10.1103/7741-585p
15. V. P. Gonçalves, G. Sampaio dos Santos and C. R. Sena, "Inclusive heavy quark photoproduction in pp, pPb and $PbPb$ collisions at Run 2 LHC energies," Nucl. Phys. A **976**, 33-45 (2018) doi:10.1016/j.nuclphysa.2018.05.002 [arXiv:1711.04497 [hep-ph]].
16. V. Chekhovsky *et al.* [CMS], "Measurement of D^0 meson photoproduction in ultraperipheral heavy ion collisions," [arXiv:2509.08626 [nucl-ex]].